Rapid Communication J. Biochem. 131, 171–173 (2002)

Structure Determination of the Constitutive 20S Proteasome from Bovine Liver at 2.75 Å Resolution[1]

Masaki Unno,[*] Tsunehiro Mizushima,[*,†] Yukio Morimoto,[‡] Yoshikazu Tomisugi,[§] Keiji Tanaka,[‖] Noritake Yasuoka,[‡] and Tomitake Tsukihara[*,2]

[*]Institute for Protein Research, Osaka University, 3-2 Yamadaoka, Suita, Osaka 565-0871; [†]"Structure and Function of Biomolecules," PRESTO, JST; [‡]Faculty of Science, Himeji Institute of Technology, 3-2-1 Kohto, Kamigori, Hyogo 678-1297; [§]The Pharmaceutical Department, Kumamoto University, 5-1 Oehonmachi, Kumamoto, Kumamoto 862-0973; and [‖]The Tokyo Metropolitan Institute of Medical Science, 3-18-22 Honkomagome, Bunkyo-ku, Tokyo 113-8613

Received November 20, 2001; accepted December 15, 2001

The crystal structure of the 20S proteasome from bovine liver was determined by the molecular replacement method using the structure of the 20S proteasome from the yeast *Saccharomyces cerevisiae*. The initial phases were refined by density modification coupled with non-crystallographic symmetry averaging. The structural model was refined with the program CNS. The final *R*-factor and R_{free} were 0.25 and 0.29, respectively. The constitutive proteasome without any contamination by the immunoproteasome was identified in the crystal structure.

Key words: constitutive proteasome, crystal structure, mammalian proteasome.

The proteasome, a multisubunit proteolytic complex, is involved in various biological processes (*1*). It consists of a central core particle (equivalent to the 20S proteasome) and two terminal regulatory particles, termed PA700, that are attached to the ends of the central portion in opposite orientations to form the enzymatically active 26S proteasome (*2, 3*). The 26S proteasome breaks down polyubiquitinated substrates into short peptides in an ATP-dependent manner (*4, 5*). The eukaryotic 20S proteasome with a molecular weight of about 700 kDa is the catalytic portion of the 26S proteasome, and can degrade unfolded proteins ATP-independently (*1, 6*). The 20S proteasome from *Thermoplasma acidophilum* consists of two subunit species (α and β), and is composed of 28 subunits arranged in a particle as four homo-heptameric rings, $\alpha_7\beta_7\beta_7\alpha_7$, with D7 symmetry (*7*). The yeast 20S proteasome is composed of two copies each of 14 different subunits, seven distinct α- and seven distinct β-type subunits. Each α- and β-type subunit of the eukaryotic 20S proteasome is similar to the α- and β-subunits of the *T. acidophilum* proteasome in amino acid sequence, respectively. These subunits exhibit a unique location, $(\alpha1\text{-}\alpha7, \beta1\text{-}\beta7)_2$, with C2 symmetry (*8*). The subunit naming proposed by Groll *et al.* (*8*) is followed in this paper.

Mammals possess seven different α and 10 different β proteasome subunit genes (*2, 6, 9*). The identity ratios between the corresponding subunits of the human and yeast proteasomes are in the range of 42.5 to 63.7% (*10*). Three β subunits, β1i, β2i, and β5i, are induced by a major immunomodulatory cytokine, γ-interferon (*11–15*). All three inducible subunits are catalytically active and replace constitutive active subunits β1, β2, and β5, respectively. In higher eukaryotes, the 20S proteasome containing the three inducible subunits, β1i, β2i, and β5i, is called the immunoproteasome, which is responsible for immunological processing of intracellular antigens. The liver produces both the constitutive and inducible subunits (*16, 17*). The sequence identities of the human β1i, β2i, and β5i subunits compared to human β1, β2, and β5 are 59.2, 57.7, and 68.6%, respectively. It is not known whether the pure constitutive 20S proteasome without any contamination by the inducible subunits exists or not.

We are currently engaged in crystal structural analysis of the 20S proteasome from bovine liver in order to elucidate the structure-function relationships and structural organization of the mammalian proteasome. The enzyme is crystallized in three different forms (*18, 19*). The X-ray structure analysis of an orthorombic form II crystal at 2.75 Å resolution will be described in this paper.

The isolation, purification and crystallization of the 20S proteasome were performed by a method previously described (*18, 19*). Diffraction data were collected at BL41XU of the SPring-8 using a 186 mm Mar CCD detector with a crystal-to-detector distance of 220 mm. The wavelength of synchrotron radiation was 1.00 Å. The oscillation angle for each shot was 0.5°. The X-ray intensities were evaluated using the program MOSFLM (*20*) and were scaled with the program SCALA of CCP4 (*21*). The crystal belonged to space group $P2_12_12_1$ with cell dimensions of a = 315.7 Å, b = 205.9 Å, and c = 116.0 Å. It was equivalent to the orthorombic form II crystal in the previous paper (*19*) judging from the cell dimensions and intensity distribution. The

[1] This work was partly supported by Grants-in-Aid for JSPS fellows to M.U. from the Ministry of Education, Science, Sports, and Culture, and by a Grant-in-Aid for "Research for the Future" Program from the Japan Society for the Promotion of Science (JSPS-RFTF-96L00503 to T.T.). This research was performed with the approval of SPring-8, Institute of Physical and Chemical Research (RIKEN) and Institute for Protein Research (Proposals 2000B0083-NL-np and 1999A0377-NL-np for BL41XU, and C01A44XU-7143-N and C01B-44XU-7143-N for BL44XU), and the Photon Factory Advisory Committee, and the National Laboratory for High Energy Physics, Japan (Proposal 98G-149).

[2] To whom correspondence should be addressed. Tel:+81-6-6879-8604, Fax: +81-6-6879-8606, E-mail: tsuki@protein.osaka-u.ac.jp

Abbreviation: NCS, non-crystallographic symmetry.

numbers of observed reflections and independent reflections were 733,250 and 189,429 between 100 and 2.75 Å spacing, respectively. The completeness, averaged $I/\sigma(I)$, and R_{merge} were 96.3, 5.6, and 9.5%, respectively, where $R_{merge} = \Sigma_{hi} |I_{hi}-\langle I_{hi}\rangle| / \Sigma \langle I_h \rangle$, I_{hi} is the observed intensity, and $\langle I_h \rangle$ is the average intensity over equivalent measurements. Those for the highest resolution shell between 2.82 and 2.75 Å were 70.0, 1.8, and 40.6%, respectively.

Assuming one molecule with the $(\alpha 1\text{-}\alpha 7, \beta 1\text{-}\beta 7)_2$ structure in the unit cell, V_m was estimated to be 2.62 Å^3/Da, *i.e.* in the acceptable range for protein crystals (*22*). A self-rotation function was calculated using the observed reflections between 20 and 5 Å resolution with the program POLARRFN in CCP4 (*21*). No isolated peak implicating a non-crystallographic twofold axis was detected in the contour map. A broad ridge of the rotation function along $\phi = 90°$ suggested that one two-fold axis and six quasi two-fold axes within the $(\alpha 1\text{-}\alpha 7, \beta 1\text{-}\beta 7)_2$ were in the *b*-*c* plane. The Patterson functions calculated at 20, 10, and 5 Å resolution exhibited no significant peak in any Harker section. The rotation function and the Patterson function suggested that the two-fold axis within the 20S proteasome was in the *b*-*c* plane, and inclined from both the *b* and *c*-axes. The cross-rotation function calculation and molecular replacement analysis were performed with the program X-PLOR (*23*) using the yeast 20S proteasome truncated to polyalanine as a search model. The cross-rotation function showed a two-fold axis within the truncated 20S proteasome model on the local twofold axis at ($\varphi = 80°$, $\phi = 90°$, and $\kappa = 180°$) in the *b*-*c* plane, as suggested by the self-rotation function. The translation function gave a unique solution of (0.082, 0.127, 0.431) in fractional coordinates. The rotation and translation parameters were refined by rigid body refinement using the observed reflections between 20 and 4 Å resolution (*24*). An *R*-factor, $R = \Sigma_h |F_h(\text{obs})-F_h(\text{calc})| / \Sigma_h F_h(\text{obs})$, in the refinement converged to 44.8% at 4 Å resolu-

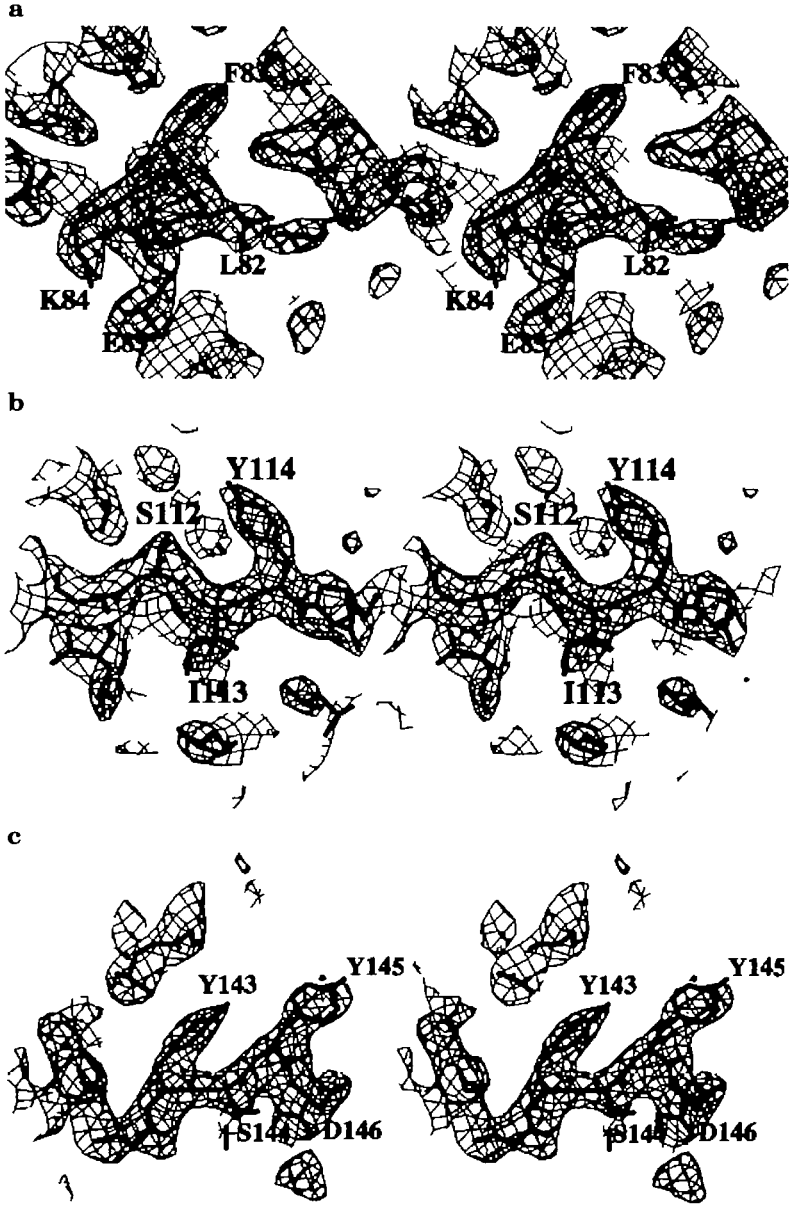

Fig. 1. **Structural models of subunits β1, β2, and β5 superposed on composite omit maps ($2F_o$-F_c) contoured at 1.5 σ are depicted as stereoscopic pairs.** The atomic parameters around the polypeptide segments were excluded from several cycles of the refinement prior to the electron density calculation to avoid biased electron density distribution for these regions. (a) The amino acid sequence of Leu-Phe-Lys-Glu for 82–85 of subunit β1 was clearly distinguished from Val-Val-Arg-Asn of β1i in the electron density map. (b) Ser-Ile-Tyr for 112–114 of subunit β2 exhibiting a β structure was superposed well on the electron density map. The corresponding amino acid sequence of Gly-Val-His of subunit β2i was not accommodated in the electron density cages. (c) Tyr-Ser-Tyr-Asp from 143 to 146 of subunit β5 was fitted well to the electron density map. Arg144-Pro145 of subunit β5i was not suitable for the map.

tion. The initial phases were calculated at a 5 Å resolution with atomic parameters obtained by means of the refinement. Further phase extension and refinement were carried out by density modification coupled with non-crystallographic symmetry (NCS) averaging with the program DM (*25*) in CCP4. At the final stage of the phase extension, the correlation coefficient and R_{free} were 0.890 and 0.285, respectively, where R_{free} is the R-factor determined for the 5% of reflections that were excluded from the density modification procedure. Model building was performed using the program TURBO-FRODO (*26*). Since those of the bovine enzyme were not known, the amino acid sequences of the human proteasome were used for the model building. Most parts of the electron density map were so clear that side chains were unambiguously assigned, but small parts, mostly in α subunits, were too poor to build side chain structures. Alanine residues were left at these parts with poor electron density. Out of the 6,454 amino acid residues, the side chain structures of 5,980 residues were assigned in the electron density map, 332 residues being left as alanine residues. Since some N-termini and C-termini lost electron density, structural models of these 142 residues were not built.

The NCS restraint of (φ = 78.4°, ϕ = 91.4°, and κ = 180.0°) was imposed on the whole molecule except for the residues from 40 to 43 and from 49 to 54 of subunit α2, and those from 236 to 241 of subunit α6 during the refinement with the program CNS (*27*). All the residues assigned except for the 91st residue of the β2 subunit were consistent with those of the human sequences. Glu91 of human β2 was replaced by an Arg residue in the bovine β2 subunit, judging from the electron density map. The final R-factor and R_{free} were 25.0 and 29.4%, respectively. Out of 5,027 non-glycine residues, only 7 (0.1%) are in the disallowed region, 71 (1.4%) in the generously allowed regions, 725 (14.4%) in the additional allowed regions, and 4,224 (84.0%) in the most favoured regions in the Ramachandran plot (*28*). The electron density map clearly distinguished the constitutive subunits from the γ-interferon inducible ones, as shown in Fig. 1, a, b, and c. The B-factors of the residues that are replaced by different amino acids in the inducible subunits were as low as those of the other residues of β subunits. Consequently, the constitutive proteasome without any contamination by the inducible subunits was identified in the crystal structure of the liver 20S proteasome. This X-ray structure of the bovine 20S proteasome proved that the yeast and mammalian proteasomes have the same subunit arrangement. The atomic parameters of the entire molecule and structure factors have been deposited in the Protein Data Bank under accession codes 1IRU and rIRUsf.ent, respectively.

REFERENCES

1. Coux, O., Tanaka, K., and Goldberg, A.L. (1996) Structure and functions of the 20S and 26S proteasomes. *Annu. Rev. Biochem.* **65**, 801–847
2. Baumeister, W., Walz, J., Zuhl, F., and Seemuler, E. (1998) The proteasome: Paradigm of a self-compartmentalizing protease. *Cell* **92**, 367–380
3. DeMartino, G.N. and Slaughter, C.A. (1999) The proteasome, a novel protease regulated by multiple mechanisms. *J. Biol. Chem.* **274**, 22123–22126
4. Hershko, A. and Ciechanover, A. (1998) The ubiquitin system. *Annu. Rev. Biochem.* **67**, 425–479
5. Pickart, C.M. (2001) Mechanisms underlying ubiquitination. *Annu. Rev. Biochem.* **70**, 503–533
6. Bochtler, M., Ditzel, L., Groll, M., Hartmann, C., and Huber, R. (1999) The proteasome. *Annu. Rev. Biophys. Biomol. Struct.* **28**, 295–317
7. Löwe, J., Stock, D., Jap, B., Zwickl, P., Baumeister, W., and Huber, R. (1995) Crystal structure of the 20S proteasome from the archaeon *T. acidphilum* at 3.4 Å resolution. *Science* **268**, 533–539
8. Groll, M. Ditzel, L., Löwe, J., Stock, D., Bochtler, M., Bartunik, H.D., and Huber, R. (1997) Structure of 20S proteasome from yeast at 2.4 Å resolution. *Nature* **386**, 463–471
9. Tanaka, K. (1998) Molecular biology of the proteasome. *Biochem. Biophys. Res. Commun.* **247**, 537–541
10. Bairoch, A. and Apweiler, R. (2000) The SWISS-PROT protein sequence database and its supplement TrEMBL in 2000. *Nucleic Acids Res.* **28**, 45–48
11. Monaco, J.J. and Nandi, D. (1995) The genetics of proteasomes and antigen processing. *Annu. Rev. Genet.* **29**, 729–754
12. Tanaka, K. and Kasahara, M. (1998). The MHC class I ligand-generating system: roles of immunoproteasomes and the interferon-γ-inducible proteasome activator PA28. *Immunol. Rev.* **163**, 161–176
13. Fruh, K. and Yang, Y. (1999). Antigen presentation by MHC class I and its regulation by interferon γ. *Curr. Opin. Immunol.* **11**, 76–81
14. Rock, K.L. and Goldberg, A.L. (1999). Degradation of cell proteins and the generation of MHC class I-presented peptides. *Annu. Rev. Immunol.* **17**, 739–779
15. Kloetzel, P.M. (2001). Antigen processing by the proteasome. *Nat. Rev.* **2**, 179–187
16. Eleuteri, A.M., Kohanski, R.A., Cardozo, C., and Orlowski, M. (1997) Bovine spleen multicatalytic proteinase complex (proteasome). Replacement of X, Y and Z subunits by LMP7, LMP2 and MECL1 and changes in properties and specificity. *J. Biol. Chem.* **272**, 11824–11831
17. Noda, C., Tanahashi, N., Shimbara, N., Hendil, K.B., and Tanaka, K. (2000) Tissue distribution of constitutive proteasomes, immunoproteasomes, and PA28 in rats. *Biochem. Biophys. Res. Commun.* **277**, 348–354
18. Morimoto, Y., Mizushima, T., Yagi, Y., Tanahashi, N., Tanaka, K., Ichihara, A., and Tsukihara, T. (1995) Ordered structure of the crystallized bovine 20S proteasome. *J. Biochem.* **117**, 471–474
19. Tomisugi, Y., Unno, M., Mizushima, T., Morimoto, Y., Tanahashi, N., Tanaka, K., Tsukihara, T., and Yasuoka, N. (2000) New crystal forms and low resolution structure analysis of 20S proteasome from bovine liver. *J. Biochem.* **127**, 941–943
20. Leslie, A.G.W. (1999) Integration of macromolecular diffraction data. *Acta Cryst. D* **55**, 1696–1702
21. Collaborative Computational Project, Number 4. (1994) The CCP4 suite: programs for protein crystallography. *Acta Crystallogr. D* **50**, 760–763
22. Matthews, B.W. (1968) Solvent content of protein crystals. *J. Mol. Biol.* **33**, 491–497
23. Brunger, A.T. (1992) *X-PLOR Version 3.1. A System for X-Ray Crystallography and NMR, Yale University Press*, New Haven and London
24. Head-Gordon, T. and Brooks, C.L. (1991) Virtual rigid body dynamics. *Biopolymers* **31**, 77–100
25. Cowtan, K. (1994) Joint CCP4 and ESF-EACBM Newsletter on Protein *Crystallography*, **31**, 34–38
26. Jones, T.A. (1978) A graphics model building and refinement system for macromolecules. *J. Appl. Cryst.* **11**, 268–272
27. Brunger, A.T., Adams, P.D., Clore, G.M., DeLano, W.L., Gros, P., Grosse-Kunstleve, R.W., Jiang, J.S., Kuszewski, J., Nilges, M., and Pannu, N.S. (1998) Crystallography & NMR system: a new software suite for macromolecular structure determination. *Acta Crystallogr. D* **54**, 905–921
28. Ramakrishnan, C. and Ramachandran, G.N. (1965) Stereochemical criteria for polypeptide and protein chain conformations. II. Allowed conformations for a pair of peptide units. *Biophys. J.* **5**, 909–993